INTERNATIONAL JOURNAL FOR NUMERICAL METHODS IN ENGINEERING
Int. J. Numer. Meth. Engng 2010; **82**:917–938
Published online 3 December 2009 in Wiley InterScience (www.interscience.wiley.com). DOI: 10.1002/nme.2804

An edge-based smoothed finite element method for primal–dual shakedown analysis of structures

Thanh Ngoc Tran[1,2,*,†], G. R. Liu[1,3], H. Nguyen-Xuan[3,4] and T. Nguyen-Thoi[1,4]

[1]*Center for Advanced Computations in Engineering Sciences (ACES), Department of Mechanical Engineering, National University of Singapore, 9 Engineering Drive 1, Singapore 117576, Singapore*
[2]*Faculty of Civil Engineering, Hanoi Architectural University, km 10 Nguyen Trai Str., Thanh Xuan Dist., Hanoi, Vietnam*
[3]*Singapore-MIT Alliance (SMA), E4-04-10, 4 Engineering Drive 3, Singapore 117576, Singapore*
[4]*Department of Mechanics, Faculty of Mathematics and Computer Science, University of Science HCM, Vietnam*

SUMMARY

An edge-based smoothed finite element method (ES-FEM) using three-node linear triangular elements was recently proposed to significantly improve the accuracy and convergence rate of the standard finite element formulation for static, free and forced vibration analyses of solids. In this paper, ES-FEM is further extended for limit and shakedown analyses of structures. A primal–dual algorithm based upon the von Mises yield criterion and a non-linear optimization procedure is used to compute both the upper and lower bounds of the plastic collapse limit and the shakedown limit. In the ES-FEM, compatible strains are smoothed over the smoothing domains associated with edges of elements. Using constant smoothing function, only one Gaussian point is required for each smoothing domain ensuring that the total number of variables in the resulting optimization problem is kept to a minimum compared with standard finite element formulation. Three benchmark problems are presented to show the stability and accuracy of solutions obtained by the present method. Copyright © 2009 John Wiley & Sons, Ltd.

Received 2 May 2009; Revised 14 October 2009; Accepted 25 October 2009

KEY WORDS: limit analysis; shakedown analysis; duality; non-linear programming; edge-based smoothed finite element method (ES-FEM); strain smoothing

*Correspondence to: Thanh Ngoc Tran, Center for Advanced Computations in Engineering Sciences (ACES), Department of Mechanical Engineering, National University of Singapore, 9 Engineering Drive 1, Singapore 117576, Singapore.
†E-mail: tran@fh-aachen.de

Contract/grant sponsor: A*Star, Singapore; contract/grant number: 052 101 0048
Contract/grant sponsor: State Key Laboratory of Advanced Technology of Design and Manufacturing for Vehicle Body, Hunan University, P.R.China; contract/grant number: 40915001

1. INTRODUCTION

Inelastic structures subjected to variable repeated or cyclic loading may work in four different regimes, which are presented in the Bree-diagram (Figure 1, [1]) together with the evolution of the structural response: elastic, shakedown (adaptation), inadaptation (non-shakedown) and limit (ultimate) state. In the elastic regime, there are no plastic effects at all, whereas in the adaptation regime, the plastic effects are restricted to the initial loading cycles and then they are followed by asymptotically elastic behaviour. Both regimes are considered as safe working ones and they constitute a foundation for the structural design. We do not consider elastic failure, such as buckling or high-cycle fatigue here. The inadaptation phenomena, such as low-cycle fatigue and/or ratchetting should be avoided since they lead to a rapid structural failure. At the limit load, the structure looses instantaneously its load bearing capacity. Theoretically, these limits may be found by a complete elasto-plastic analysis, but in most cases the task is extremely cumbersome. Limit and shakedown analyses calculate directly the load-carrying capacity or the maximum load intensities that the structure is able to support. The structural shakedown takes place due to development of permanent residual stresses which were imposed on the actual stresses to shift them towards purely elastic behaviour. Residual stresses are a result of kinematically inadmissible plastic strains introduced to the structure by overloads. They clear out effects of all preceding smaller loads. They also avoid any plastic effects in the future provided that the loads are smaller than the initial overload. Therefore, in limit and shakedown analyses the knowledge of the exact load history is

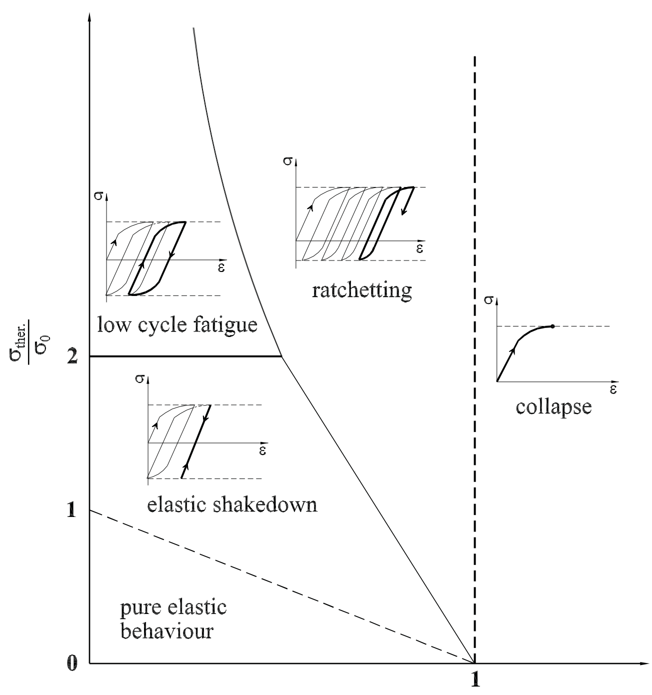

Figure 1. Bree-diagram of a pressurized thin wall tube under thermal and mechanical loads.

DOI: 10.1002/nme

not necessary. Only the maximum loads (limits) count and the envelopes of load domain should be taken into consideration.

The result of load factors in the structural shakedown analysis can be obtained from upper bound and lower bound approaches. The upper bound shakedown analysis is based on Koiter's kinametic theorem to determine the minimum load factor for non-shakedown, see e.g. [2, 3]. The strategy of computation is initiated from the unsafe region to calculate the exterior approximation of the shakedown load domain by supposing a kinematically admissible failure mechanism. On the contrary, the lower bound shakedown analysis is based on Melan's static theorem, and the strategy of computation begins from the safe region by supposing a statically admissible stress field to determine the maximum load factor for shakedown, see e.g. [4, 5]. Duality between these two bounds was proved by the flow rule including two main points: (1) the strain rate vector is proportional to the gradient of the yield function and (2) the plastic multiplier can be non-negative only at points where the yield function equals to zero. Recently, Andersen *et al.* [6] developed an excellent primal–dual interior-point algorithm to minimize a sum of Euclidean norms. They showed that the application of the duality combining with Newton method may lead to very accurate results in limit analysis. Vu *et al.* [7] then presented a primal–dual algorithm for shakedown analysis with the use of kinematically admissible finite elements. By using Newton-like iteration, it was found that upper and lower bounds of the load factor converge rapidly to the accurate solution of shakedown limit. However, it is highly recommended that the primal–dual algorithm should not be used with linear finite elements [8]. Therefore, the application of standard FEM for the above algorithm results in a large number of total optimization variables, which needs much computational effort. Possible alternative is an iterative method proposed by Garcea *et al.* [9]. In their paper, the adopted FEM element, which can be regarded as mixed one assuming a constant stress interpolation in each edge-area partition, can represent an effective compromise between accuracy and numerical efficiency in plasticity problems.

Recently, some stabilization techniques such as the strain smoothing technique [10], stable particle technique [11], cracking particle [12], external enrichment [13, 14], etc. have been proposed to stabilize meshfree methods. Liu *et al.* has generalized the gradient (strain) smoothing technique [10] and applied it in the meshfree context to formulate the node-based smoothed point interpolation method (NS-PIM or LC-PIM) [15, 16] and the node-based smoothed radial point interpolation method (NS-RPIM or LC-RPIM) [17]. Applying the same idea to the FEM, a cell/element-based smoothed finite element method (SFEM or CS-FEM) [10, 11, 18, 19] and a node-based smoothed finite element method (NS-FEM) [20] have also been formulated.

CS-FEM is formulated using smoothing domains located inside the elements and proven effectively in solving 2D solid mechanics problems by using a proper number of smoothing cells in each element (for example four smoothing cells) [18, 19, 21, 22]. The CS-FEM has also been extended for general n-sided polygonal elements (nSFEM or nCS-FEM) [23], dynamic analyses [24], incompressible materials using selective integration [25, 26], plate and shell analyses [27–30], and further extended for the extended finite element method (XFEM) to solve fracture mechanics problems in 2D continuum and plates [31].

NS-FEM uses node-based smoothing domains associated from the predefined parts of all adjacent elements around the node. It can provide upper bound solutions in the strain energy and is also immune from volumetric locking naturally. However, the NS-FEM was found temporally instable, and can not be applied directly to dynamic problems. The NS-FEM has been developed for adaptive analysis [32] and extended to formulate the alpha-FEM [33], which combines both NS-FEM with FEM.

DOI: 10.1002/nme

To overcome such a temporal instability, Liu *et al.* [34] have very recently proposed an edge-based smoothed finite element method (ES-FEM) for static, free and forced vibration analyses of solid 2D mechanics problems. Intensive numerical results demonstrated that ES-FEM possesses the following excellent properties: (1) ES-FEM are much more accurate than the linear triangular elements of FEM (FEM-T3) and often found even more accurate than those of the FEM using quadrilateral elements (FEM-Q4) with the same sets of nodes; (2) there are no spurious non-zeros energy modes found in free vibration analyses and hence the method is also temporally stable, which shows that numerical results are stable in the time marching in forced vibration analyses; and (3) no additional degree of freedom at nodes is used and the computational efficiency is better than the FEM using the same sets of nodes. The ES-FEM was then developed for static and eigenvalue analysis of two-dimensional piezoelectric structures [35], and was also extended to the face-based smoothed finite element method (FS-FEM) [36, 37] for solving 3D linear and non-linear solid mechanics problems.

Note that the above-mentioned smoothed FEM (S-FEM) models are variationally consistent based on the modified two-field Hellinger–Reissner principle [22, 34, 36]. However, although the two-field Hellinger–Reissner principle is used, the S-FEM models have only the displacements as unknowns. Therefore, it is very much different from the so-called mixed FEM formulation [38–41], where stresses (or strains) are usually also unknowns.

In this paper, the ES-FEM is further extended for limit and shakedown analyses of structures made of elastic-perfectly plastic material. A primal–dual algorithm based upon the von Mises yield criterion and a non-linear optimization procedure is used to compute simultaneously both the upper and lower bounds of the plastic collapse limit and the shakedown limit. In the ES-FEM, compatible strains are smoothed over the smoothing domains associated with edges of elements. Using constant smoothing function, only one Gaussian point is required for each domain ensuring that the total number of variables in the resulting optimization problem is kept to a minimum compared with standard finite element formulation. Two benchmark problems are presented to show the stability and accuracy of solutions obtained by the present method.

2. THE FORMULATION OF THE ES-FEM

Similar to the FEM, the ES-FEM also uses a mesh of elements. When three-node triangular elements are used, the shape functions used in the ES-FEM are also identical to those in the FEM, and hence the displacement field in the ES-FEM is also ensured to be continuous on the whole problem domain. However, the ES-FEM does not use the compatible strain fields $\boldsymbol{\varepsilon}=\nabla_s \mathbf{u}$ but strains 'smoothed' over local smoothing domains. These local smoothing domains are constructed based on edges of the elements such that $\Omega=\bigcup_{k=1}^{N_e}\Omega^{(k)}$ and $\Omega^{(i)}\cap\Omega^{(j)}=\emptyset$ for $i\neq j$, in which N_e is the total number of edges of all elements in the entire problem domain. For triangular elements, the smoothing domain $\Omega^{(k)}$ associated with the edge k is created by connecting two end-points of the edge to centroids of adjacent elements as shown in Figure 2. Smoothed strains are now defined by the following operation

$$\tilde{\boldsymbol{\varepsilon}}_k=\int_{\Omega^{(k)}}\boldsymbol{\varepsilon}(\mathbf{x})\Phi_k(\mathbf{x})\,\mathrm{d}\Omega=\int_{\Omega^{(k)}}\nabla_s\mathbf{u}(\mathbf{x})\Phi_k(\mathbf{x})\,\mathrm{d}\Omega \tag{1}$$

DOI: 10.1002/nme

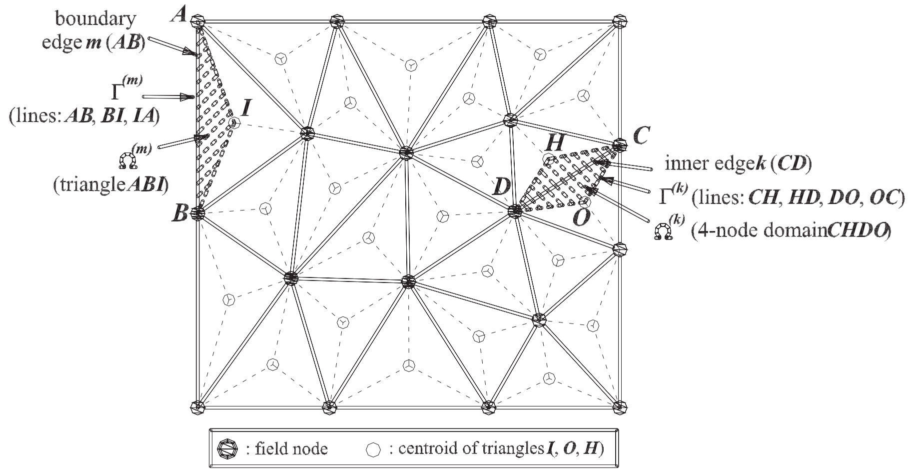

Figure 2. Division of domain into triangular element and smoothing cells $\Omega^{(k)}$ connected to edge k of triangular elements.

where $\Phi_k(\mathbf{x})$ is a given smoothing function that satisfies unity property

$$\int_{\Omega^{(k)}} \Phi_k(\mathbf{x})\,\mathrm{d}\Omega = 1 \tag{2}$$

By using the constant smoothing function

$$\Phi_k(\mathbf{x}) = \begin{cases} 1/A^{(k)}, & \mathbf{x} \in \Omega^{(k)}, \\ 0, & \mathbf{x} \notin \Omega^{(k)}, \end{cases} \tag{3}$$

where $A^{(k)}$ is the area of the smoothing domain $\Omega^{(k)}$. In term of nodal displacement vectors $\mathbf{d}_I$, the smoothing strains can be written as

$$\tilde{\boldsymbol{\varepsilon}}_k = \sum_{I \in N_n^{(k)}} \tilde{\mathbf{B}}_I(\mathbf{x}_k)\mathbf{d}_I, \tag{4}$$

where $N_n^{(k)}$ is the set of all nodes of the elements that share the common edge k (for example, $N_n^{(k)} = \{A, B, C\}$ for boundary edge m and $N_n^{(k)} = \{D, E, F, G\}$ for inner edge k as shown in Figure 2, and $\tilde{\mathbf{B}}_I(\mathbf{x}_k)$ is the smoothed strain–displacement matrix on the domain $\Omega^{(k)}$ which is calculated numerically by an assembly process similarly as in the standard FEM

$$\tilde{\mathbf{B}}_I(\mathbf{x}_k) = \frac{1}{A^{(k)}} \sum_{j=1}^{N_e^{(k)}} \frac{1}{3} A_e^{(j)} \mathbf{B}_j, \tag{5}$$

in which $N_e^{(k)}$ is the total number of elements around the edge k ($N_e^{(k)} = 1$ for the boundary edges and $N_e^{(k)} = 2$ for the inner edges as shown in Figure 2, and $A_e^{(j)}$, $\mathbf{B}_j$ are the area and the compatible strain gradient matrix of the jth element around the edge k, respectively. When linear triangular elements T3 are used, the entries of $\mathbf{B}_j$ and therefore of $\tilde{\mathbf{B}}_I(\mathbf{x}_k)$ are also constants.

The smoothed domain stiffness matrix is then calculated by

$$\tilde{\mathbf{K}}_{(k)} = \int_{\Omega^{(k)}} \tilde{\mathbf{B}}_I^{\mathrm{T}} \mathbf{E} \tilde{\mathbf{B}}_I \, \mathrm{d}\Omega = A^{(k)} \tilde{\mathbf{B}}_I^{\mathrm{T}} \mathbf{E} \tilde{\mathbf{B}}_I \tag{6}$$

where $\mathbf{E}$ is the matrix of material constants. The global stiffness matrix is then assembled from all domain stiffness matrices $\tilde{\mathbf{K}}_{(k)}$ by a similar process as in the FEM. Note that due to the smoothed strains $\tilde{\boldsymbol{\varepsilon}}_k$ in (1), the stresses obtained from $\tilde{\boldsymbol{\varepsilon}}_k$ are also constant in the smoothing domain.

Note that the FEM model in the standard version is displacement-based and fully compatible. The FEM model is hence stiffer than the real model, and the numerical results obtained are under-estimated compared with the exact results. In the ES-FEM, the smoothed strain, instead the compatible strain, is used on the smoothing domains. The ES-FEM-T3 is hence softer and more accurate than FEM-T3. The numerical results observed from reference [34] even show that ES-FEM is often more accurate than FEM-Q4.

Also note that the ES-FEM is both spatially and temporally stable, and should have no spurious non-zero energy modes, and hence is well suited for the dynamic analyses. These were shown clearly by theoretical analysis and numerical results of both static and dynamics problems in Reference [34].

3. LIMIT AND SHAKEDOWN ANALYSIS BASED ON ES-FEM

Consider a convex polyhedral load domain $\mathscr{L}$ and a special loading path consisting of all load vertices $\hat{P}_i$ $(i = 1, \ldots, m)$ of $\mathscr{L}$. At each load vertex, the kinematical condition may not be satisfied, however the accumulated strains over a load cycle $\Delta\tilde{\boldsymbol{\varepsilon}}$ must be kinematically compatible. Let the fictitious elastic stress vector be $\boldsymbol{\sigma}^E$. According to Koiter's theorem, the upper bound shakedown limit, which is the smaller one of the low cycle fatigue limit and the ratcheting limit, may be found by the following minimization

$$\alpha^+ = \min \sum_{i=1}^{m} \int_{\Omega} D^p(\dot{\tilde{\boldsymbol{\varepsilon}}}_{ik}) \, \mathrm{d}\Omega \tag{7a}$$

$$\text{s.t.} \begin{cases} \Delta\tilde{\boldsymbol{\varepsilon}}_k = \sum\limits_{i=1}^{m} \dot{\tilde{\boldsymbol{\varepsilon}}}_{ik} = \nabla_s(\Delta\mathbf{u}_k) \quad \text{in } \Omega & \text{(7b)} \\ \Delta\mathbf{u}_k = 0 \quad \text{on } \partial\Omega_u & \text{(7c)} \\ \mathbf{D}_v \dot{\tilde{\boldsymbol{\varepsilon}}}_{ik} = \mathbf{0}, & \text{(7d)} \\ \sum\limits_{i=1}^{m} \int_{\Omega} \dot{\tilde{\boldsymbol{\varepsilon}}}_{ik}^{\mathrm{T}} \boldsymbol{\sigma}_k^E(x, \hat{P}_i) \, \mathrm{d}\Omega = 1, & \text{(7e)} \end{cases}$$

in which $D^p(\dot{\tilde{\boldsymbol{\varepsilon}}}_{ik})$ is the plastic dissipation power per unit domain. The third constraint (Equation (7d)) ensures that the incompressibility condition must be satisfied on all smoothing domains $\Omega^{(k)}$

DOI: 10.1002/nme

and at all load vertices i. For plane strain problems, $\mathbf{D}_v$ has the form:

$$\mathbf{D}_v = \begin{bmatrix} 1 & 1 & 0 \\ 1 & 1 & 0 \\ 0 & 0 & 0 \end{bmatrix}. \tag{8}$$

Equation (7e) implies the normalized condition, i.e. the external load power is equal to one. By discretizing the entire problem domain into smoothing domains, applying the strain smoothing technique described in Section 2 and using von Mises yield criterion, Equation (7) can be rewritten in the following form:

$$\alpha^{+} = \min \sum_{i=1}^{m} \sum_{k=1}^{N_{\mathrm{e}}} A^{(k)} \sqrt{\frac{2}{3}} \sigma_y \sqrt{\dot{\tilde{\boldsymbol{\varepsilon}}}_{ik}^{\mathrm{T}} \mathbf{D} \dot{\tilde{\boldsymbol{\varepsilon}}}_{ik} + \varepsilon_0^2} \tag{9a}$$

$$\text{s.t.} \begin{cases} \sum_{i=1}^{m} \dot{\tilde{\boldsymbol{\varepsilon}}}_{ik} = \tilde{\mathbf{B}}_k \dot{\mathbf{u}} \quad \forall k = \overline{1, N_{\mathrm{e}}} & \text{(9b)} \\ \mathbf{D}_v \dot{\tilde{\boldsymbol{\varepsilon}}}_{ik} = \mathbf{0} \quad \forall k = \overline{1, N_{\mathrm{e}}}, \quad \forall i = \overline{1, m} & \text{(9c)} \\ \sum_{i=1}^{m} \sum_{k=1}^{N_{\mathrm{e}}} A^{(k)} \dot{\tilde{\boldsymbol{\varepsilon}}}_{ik}^{\mathrm{T}} \boldsymbol{\sigma}_{ik}^{E} = 1, & \text{(9d)} \end{cases}$$

where σ_y is yield stress and ε_0^2 is a small positive number to ensure the objective function to be differentiable everywhere. $\mathbf{D}$ is diagonal square matrix and has the following form for two-dimensional problems:

$$\mathbf{D} = \mathrm{diag}[1 \;\; 1 \;\; \tfrac{1}{2}]. \tag{10}$$

Note that the second constraint in (7) is omitted here since it will be automatically fulfilled by the algorithm. For the sake of simplicity, some new notations are introduced

$$\dot{\mathbf{e}}_{ik} = A^{(k)} \mathbf{D}^{1/2} \dot{\tilde{\boldsymbol{\varepsilon}}}_{ik}, \quad \mathbf{t}_{ik} = \mathbf{D}^{-1/2} \boldsymbol{\sigma}_{ik}^{E}, \quad \hat{\mathbf{B}}_k = A^{(k)} \mathbf{D}^{1/2} \tilde{\mathbf{B}}_k, \tag{11}$$

where $\dot{\mathbf{e}}_{ik}, \mathbf{t}_{ik}, \hat{B}_i$ are the new strain rate vector, new fictitious elastic stress vector and new strain matrix, respectively. By substituting (11) into (9), we obtain a simplified version for the upper bound shakedown analysis (primal problem)

$$\alpha^{+} = \min \sum_{i=1}^{m} \sum_{k=1}^{N_{\mathrm{e}}} \sqrt{\frac{2}{3}} \sigma_y \sqrt{\dot{\mathbf{e}}_{ik}^{\mathrm{T}} \dot{\mathbf{e}}_{ik} + \varepsilon_0^2} \tag{12a}$$

$$\text{s.t.} \begin{cases} \sum_{i=1}^{m} \dot{\mathbf{e}}_{ik} - \hat{\mathbf{B}}_k \dot{\mathbf{u}} = \mathbf{0} \quad \forall k = \overline{1, N_{\mathrm{e}}} & \text{(12b)} \\ \mathbf{D}_v \dot{\mathbf{e}}_{ik} = \mathbf{0} \quad \forall k = \overline{1, N_{\mathrm{e}}}, \quad \forall i = \overline{1, m} & \text{(12c)} \\ \sum_{i=1}^{m} \sum_{k=1}^{N_{\mathrm{e}}} \dot{\mathbf{e}}_{ik}^{\mathrm{T}} \mathbf{t}_{ik} - 1 = 0. & \text{(12d)} \end{cases}$$

The Lagrangian associated with the primal problem (12) can be written as

$$L=\sum_{k=1}^{N_e}\left\{\sum_{i=1}^{m}\sqrt{\frac{2}{3}}\sigma_y\sqrt{\dot{\mathbf{e}}_{ik}^{\mathrm{T}}\dot{\mathbf{e}}_{ik}+\varepsilon_0^2}-\sum_{i=1}^{m}\boldsymbol{\gamma}_{ik}^{\mathrm{T}}\mathbf{D}_v\dot{\mathbf{e}}_{ik}-\boldsymbol{\beta}_k^{\mathrm{T}}\left(\sum_{i=1}^{m}\dot{\mathbf{e}}_{ik}-\hat{\mathbf{B}}_k\dot{\mathbf{u}}\right)\right\}-\alpha\left(\sum_{k=1}^{N_e}\sum_{i=1}^{m}\dot{\mathbf{e}}_{ik}^{\mathrm{T}}\mathbf{t}_{ik}-1\right), \quad (13)$$

where $\boldsymbol{\gamma}_{ik}$, $\boldsymbol{\beta}_k$, α are Lagrange multipliers. The dual problem of (12) has the form

$$\max_{\boldsymbol{\gamma}_{ik},\boldsymbol{\beta}_k,\alpha}\ (\min_{\dot{\mathbf{e}}_{ik},\dot{\mathbf{u}}} L). \quad (14)$$

Since a finite solution for (12) exists, the constraints (12b)–(12d) are affine, the objective function in (12a) is convex, thus according to the strong duality theorem, there exists no gap between primal problem (12) and its dual problem (14), i.e.

$$\min_{\mathbf{h}(\dot{\mathbf{e}}_{ik},\dot{\mathbf{u}})=\mathbf{0}}\sum_{i=1}^{m}\sum_{k=1}^{N_e}\sqrt{\frac{2}{3}}\sigma_y\sqrt{\dot{\mathbf{e}}_{ik}^{\mathrm{T}}\dot{\mathbf{e}}_{ik}+\varepsilon_0^2}=\max_{\boldsymbol{\gamma}_{ik},\boldsymbol{\beta}_k,\alpha}\left(\min_{\dot{\mathbf{e}}_{ik},\dot{\mathbf{u}}} L\right), \quad (15)$$

where $\mathbf{h}(\dot{\mathbf{e}}_{ik},\dot{\mathbf{u}})=\mathbf{0}$ stands for three linear constraints (12b)–(12d). It was proved in [42] that Equation (15) satisfies if and only if $\min_{\dot{\mathbf{e}}_{ik},\dot{\mathbf{u}}} L=\alpha$, $\|\boldsymbol{\gamma}_{ik}+\boldsymbol{\beta}_k+\alpha\mathbf{t}_{ik}\|\leqslant\sqrt{\frac{2}{3}}\sigma_y$ and $\sum_{k=1}^{N_e}\hat{\mathbf{B}}_k^{\mathrm{T}}\boldsymbol{\beta}_k=\mathbf{0}$ hold. Thus, the dual problem of (12) takes the form

$$\alpha^{-}=\max\alpha \quad (16a)$$

$$\text{s.t.}\begin{cases}\|\boldsymbol{\gamma}_{ik}+\boldsymbol{\beta}_k+\alpha\mathbf{t}_{ik}\|\leqslant\sqrt{\dfrac{2}{3}}\sigma_y, & (16b)\\ \displaystyle\sum_{k=1}^{N_e}\hat{\mathbf{B}}_k^{\mathrm{T}}\boldsymbol{\beta}_k=\mathbf{0}. & (16c)\end{cases}$$

The form (16) is also exactly the discretized form of the lower bound shakedown limit which is formulated by Melan's static theorem. It is noted that when $m=1$, the formulations (12) and (16) reduce to those of limit analysis.

4. A PRIMAL–DUAL ALGORITHM FOR LIMIT AND SHAKEDOWN ANALYSIS

Dealing with the non-linear constrained optimization problem (12), an efficient technique for large-scale optimization problems that are successfully applied in [6, 8] is employed. First, a penalty method is used to eliminate two first constraints in (12) leading to a penalty function

$$P=\sum_{k=1}^{N_e}\left\{\sum_{i=1}^{m}\sqrt{\dot{\mathbf{e}}_{ik}^{\mathrm{T}}\dot{\mathbf{e}}_{ik}+\varepsilon_0^2}+\frac{c}{2}\sum_{i=1}^{m}\dot{\mathbf{e}}_{ik}^{\mathrm{T}}\mathbf{D}_v\dot{\mathbf{e}}_{ik}+\frac{c}{2}\left(\sum_{i=1}^{m}\dot{\mathbf{e}}_{ik}-\hat{\mathbf{B}}_k\dot{\mathbf{u}}\right)^{\mathrm{T}}\left(\sum_{i=1}^{m}\dot{\mathbf{e}}_{ik}-\hat{\mathbf{B}}_k\dot{\mathbf{u}}\right)\right\}, \quad (17)$$

where c is a penalty parameter such that $c\gg 1$. The corresponding Lagrangian of (12) is

$$L=P-\alpha\left(\sum_{k=1}^{N_e}\sum_{i=1}^{m}\dot{\mathbf{e}}_{ik}^{\mathrm{T}}\mathbf{t}_{ik}-1\right). \quad (18)$$

We denote

$$\begin{aligned}\boldsymbol{\gamma}_{ik} &= -c\mathbf{D}_v\dot{\mathbf{e}}_{ik},\\ \boldsymbol{\beta}_k &= -c\left(\sum_{i=1}^{m}\dot{\mathbf{e}}_{ik}-\hat{\mathbf{B}}_k\dot{\mathbf{u}}\right).\end{aligned} \tag{19}$$

Employing Newton method to solve the KKT optimality conditions of the Lagrangian in (18) and after some manipulations, one gets the following system:

$$\mathbf{K}\,\mathrm{d}\dot{\mathbf{u}} = -\mathbf{K}\dot{\mathbf{u}}+\mathbf{f}_1+\mathbf{f}_2(\alpha+\mathrm{d}\alpha), \tag{20}$$

where

$$\tilde{\mathbf{K}} = \sum_{k=1}^{N_\mathrm{e}}\hat{\mathbf{B}}_k^\mathrm{T}\mathbf{S}_k^{-1}\hat{\mathbf{B}}_k, \tag{21a}$$

$$\mathbf{f}_1 = -\sum_{k=1}^{N_\mathrm{e}}\hat{\mathbf{B}}_k^\mathrm{T}\mathbf{S}_k^{-1}\sum_{i=1}^{m}\mathbf{M}_{ik}^{-1}(\boldsymbol{\gamma}_{ik}+\boldsymbol{\beta}_k+\alpha\mathbf{t}_{ik})\frac{\dot{\mathbf{e}}_{ik}^\mathrm{T}\dot{\mathbf{e}}_{ik}}{\sqrt{\dot{\mathbf{e}}_{ik}^\mathrm{T}\dot{\mathbf{e}}_{ik}+\varepsilon_0^2}}, \tag{21b}$$

$$\mathbf{f}_2 = \sum_{k=1}^{N_\mathrm{e}}\hat{\mathbf{B}}_k^\mathrm{T}\mathbf{S}_k^{-1}\sum_{i=1}^{m}\mathbf{M}_{ik}^{-1}\sqrt{\dot{\mathbf{e}}_{ik}^\mathrm{T}\dot{\mathbf{e}}_{ik}+\varepsilon_0^2}\,\mathbf{t}_{ik}, \tag{21c}$$

and

$$\begin{aligned}\mathbf{S}_k &= \frac{\mathbf{I}}{c}+\sum_{i=1}^{m}\mathbf{M}_{ik}^{-1}\sqrt{\dot{\mathbf{e}}_{ik}^\mathrm{T}\dot{\mathbf{e}}_{ik}+\varepsilon_0^2},\\ \mathbf{M}_{ik} &= \sqrt{\frac{2}{3}}\sigma_y\mathbf{I}+(\boldsymbol{\gamma}_{ik}+\boldsymbol{\beta}_k+\alpha\mathbf{t}_{ik})\frac{\dot{\mathbf{e}}_{ik}^\mathrm{T}}{\sqrt{\dot{\mathbf{e}}_{ik}^\mathrm{T}\dot{\mathbf{e}}_{ik}+\varepsilon_0^2}}+c\sqrt{\dot{\mathbf{e}}_{ik}^\mathrm{T}\dot{\mathbf{e}}_{ik}+\varepsilon_0^2}\,\mathbf{D}_v.\end{aligned} \tag{22}$$

The system (20) with the two last terms on the right-hand side may be interpreted as the linear system arising in purely elastic computations with the global stiffness matrix $\mathbf{K}$. The matrix $\mathbf{S}_k^{-1}$ plays the role of the elastic matrix in the smoothing domains $\Omega^{(k)}$ while the vector

$$\mathbf{f} = \mathbf{f}_1+\mathbf{f}_2(\alpha+\mathrm{d}\alpha), \tag{23}$$

is considered as the vector of nodal forces applied on the structure. In order to reduce the computational costs, one can make the matrix $\mathbf{S}_k^{-1}$ symmetric by

$$\mathbf{S}_k^{-1} = \tfrac{1}{2}\{\mathbf{S}_k^{-1}+(\mathbf{S}_k^{-1})^\mathrm{T}\} \tag{24}$$

Solving system (20) by the same procedure as for the purely elastic calculation will ensure the constraint (7c) to be satisfied automatically. We have the incremental vectors of displacement, strain rate, $\boldsymbol{\gamma}_{ik}$ and $\boldsymbol{\beta}_k$ as

$$\mathrm{d}\dot{\mathbf{u}} = \mathrm{d}\dot{\mathbf{u}}_1+\mathrm{d}\dot{\mathbf{u}}_2(\alpha+\mathrm{d}\alpha), \tag{25a}$$

$$\mathrm{d}\dot{\mathbf{e}}_{ik} = (\mathrm{d}\dot{\mathbf{e}}_{ik})_1+(\mathrm{d}\dot{\mathbf{e}}_{ik})_2(\alpha+\mathrm{d}\alpha), \tag{25b}$$

$$\mathrm{d}\boldsymbol{\beta}_k = (\mathrm{d}\boldsymbol{\beta}_k)_1 + (\mathrm{d}\boldsymbol{\beta}_k)_2(\alpha+\mathrm{d}\alpha), \tag{25c}$$

$$\mathrm{d}\boldsymbol{\gamma}_{ik} = cD_v\,\mathrm{d}\dot{\mathbf{e}}_{ik}, \tag{25d}$$

where

$$\mathrm{d}\dot{\mathbf{u}}_1 = -\dot{\mathbf{u}} + \tilde{\mathbf{K}}^{-1}\mathbf{f}_1,$$

$$\mathrm{d}\dot{\mathbf{u}}_2 = \tilde{\mathbf{K}}^{-1}\mathbf{f}_2,$$

$$\begin{aligned}
(\mathrm{d}\dot{\mathbf{e}}_{ik})_1 &= \mathbf{M}_{ik}^{-1}\sqrt{\dot{\mathbf{e}}_{ik}^{\mathrm{T}}\dot{\mathbf{e}}_{ik}+\varepsilon_0^2}(\boldsymbol{\gamma}_{ik}+\boldsymbol{\beta}_k+(\mathrm{d}\boldsymbol{\beta}_k)_1)-\sqrt{\frac{2}{3}}\sigma_y\mathbf{M}_{ik}^{-1}\dot{\mathbf{e}}_{ik},\\
(\mathrm{d}\dot{\mathbf{e}}_{ik})_2 &= \mathbf{M}_{ik}^{-1}\sqrt{\dot{\mathbf{e}}_{ik}^{\mathrm{T}}\dot{\mathbf{e}}_{ik}+\varepsilon_0^2}((\mathrm{d}\boldsymbol{\beta}_k)_2-\mathbf{t}_{ik}),\\
(\mathrm{d}\boldsymbol{\beta}_k)_1 &= \mathbf{S}_k^{-1}\left\{\sum_{i=1}^{m}\mathbf{M}_{ik}^{-1}\left(\sqrt{\frac{2}{3}}\sigma_y\mathbf{I}+c\sqrt{\dot{\mathbf{e}}_{ik}^{\mathrm{T}}\dot{\mathbf{e}}_{ik}+\varepsilon_0^2}\mathbf{D}_v\right)\dot{\mathbf{e}}_{ik}+\left[\hat{\mathbf{B}}_k\mathrm{d}\dot{\mathbf{u}}_1-\left(\sum_{i=1}^{m}\dot{\mathbf{e}}_{ik}-\hat{\mathbf{B}}_k\dot{\mathbf{u}}\right)\right]\right\}+\boldsymbol{\beta}_k,\\
(\mathrm{d}\boldsymbol{\beta}_k)_2 &= \mathbf{S}_k^{-1}\left(\hat{\mathbf{B}}_k\,\mathrm{d}\dot{\mathbf{u}}_2+\sum_{i=1}^{m}\mathbf{M}_{ik}^{-1}\sqrt{\dot{\mathbf{e}}_{ik}^{\mathrm{T}}\dot{\mathbf{e}}_{ik}+\varepsilon_0^2}\mathbf{t}_{ik}\right),
\end{aligned} \tag{26}$$

and

$$(\alpha+\mathrm{d}\alpha) = \left[\frac{1-\sum_{k=1}^{N_\mathrm{e}}\sum_{i=1}^{m}\mathbf{t}_{ik}^{\mathrm{T}}(\dot{\mathbf{e}}_{ik}+(\mathrm{d}\dot{\mathbf{e}}_{ik})_1)}{\sum_{k=1}^{N_\mathrm{e}}\sum_{i=1}^{m}\mathbf{t}_{ik}^{\mathrm{T}}(\mathrm{d}\dot{\mathbf{e}}_{ik})_2}\right]. \tag{27}$$

The vectors $\mathrm{d}\dot{\mathbf{u}}$, $\mathrm{d}\dot{\mathbf{e}}_{ik}$, $\mathrm{d}\boldsymbol{\gamma}_{ik}$, $\mathrm{d}\boldsymbol{\beta}_k$ and $\mathrm{d}\alpha$ are actually Newton directions which assure that a suitable step along them will lead to a decrease of the objective function of the primal problem (12) and to an increase of the objective function of the dual problem (6). Based on (25) we can update the vectors of displacement, strain rate, $\boldsymbol{\gamma}_{ik}$, $\boldsymbol{\beta}_k$ and α. Iterating these steps may drive us to a stable set of $\dot{\mathbf{u}}$, $\dot{\mathbf{e}}_{ik}$, $\boldsymbol{\gamma}_{ik}$, $\boldsymbol{\beta}_k$ and α satisfying all conditions in (12) and (6). More details of the iterative algorithm can be found in [7].

5. NUMERICAL EXAMPLES

In this section, some numerical examples are presented to test the performance of the present primal–dual shakedown algorithm using the ES-FEM. A number of two-dimensional problems in engineering practice are considered. The three-node triangular elements (FEM-T3) were applied for structural discretization. In all numerical examples, the structures are made of elastic-perfectly plastic material. For each test case, some existing analytical and numerical solutions found in literature are briefly represented and compared.

5.1. Grooved rectangular plate subjected to varying tension and bending

We first consider a grooved rectangular plate subjected to in-plane tension p_N and bending p_M (Figure 3(a)). The load domain is defined by

$$\begin{aligned} p_M &\in [0,\sigma_y],\\ p_N &\in [0,\sigma_y]. \end{aligned} \tag{28}$$

DOI: 10.1002/nme

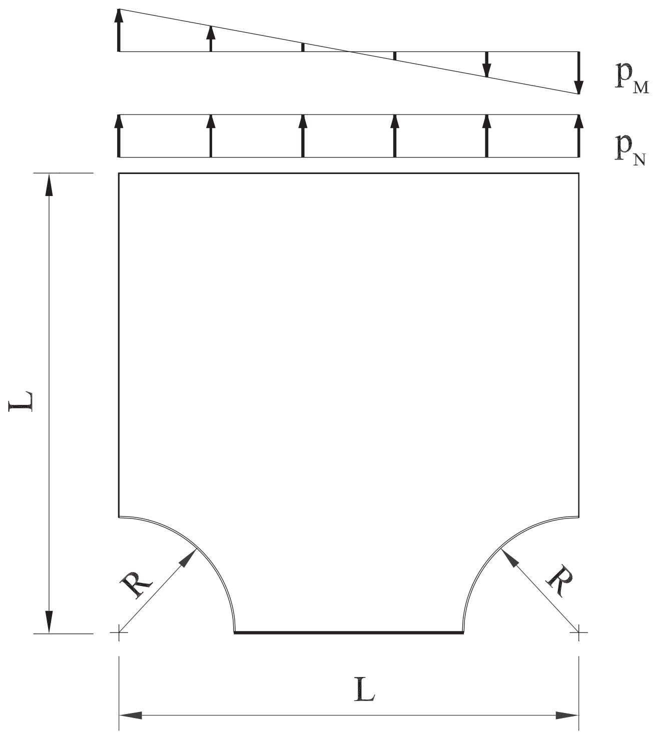

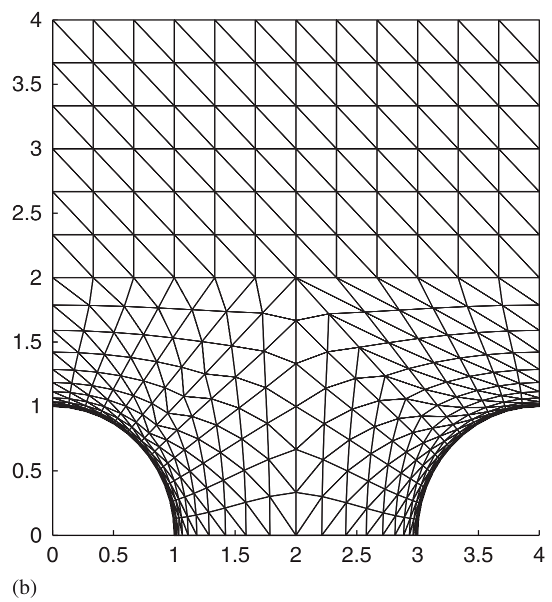

Figure 3. FE-mesh and geometrical dimensions of grooved rectangular plate.

DOI: 10.1002/nme

Table I. Limit analysis ($p_N = \sigma_y$, $p_M = 0$).

	Plane stress	Plane strain	Nature of solution	Yield criterion
Prager [43]	0.500	0.630–0.695	Analytical	Tresca
Casciaro [44]	0.568	0.699	Numerical	von Mises
Yan [45]	0.500–0.577	0.727–0.800	Analytical	von Mises
Yan [45]	0.558	0.769	Numerical	von Mises
Vu [47]	0.557	0.799–0.802	Numerical	von Mises
Tran [48]	0.572	—	Numerical	von Mises
Present	0.556	0.768	Numerical	von Mises

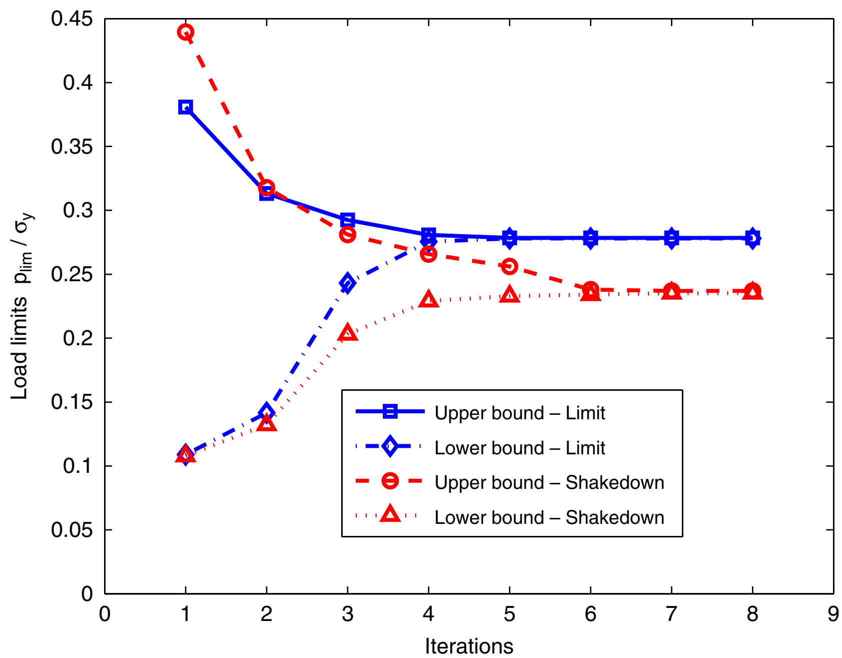

Figure 4. Grooved rectangular plate: convergence of limit and shakedown load factors.

Limit analysis of the structure was studied by Prager and Hodge [43], Casciaro and Cascini [44], Yan [45] for pure tension load $p_N \neq 0$, $p_M = 0$. Heitzer [46], Vu [47] and Tran [48] investigated the problem for the more complicated case with $p_N \neq 0$, $p_M \neq 0$. In the present analysis, the structure is modelled by 720 three-node triangular elements (T3) as shown in Figure 3(b). The following geometrical data are used: $R = 250\,\text{mm}$, $L = 4R$.

Consider the case of constant pure tension $p_N = \sigma_y$,$p_M = 0$. The results of the plastic collapse load factor are presented in Table I together with known solutions for comparison. It is seen that our ES-FEM-T3 solutions are well accordant with other existing solutions for both plane stress and plane strain assumptions.

Limit and shakedown analysis are also implemented for the case of having both in-plane tension and bending, Figure 4 shows the evolutions of limit and shakedown load factors. In the case of

DOI: 10.1002/nme

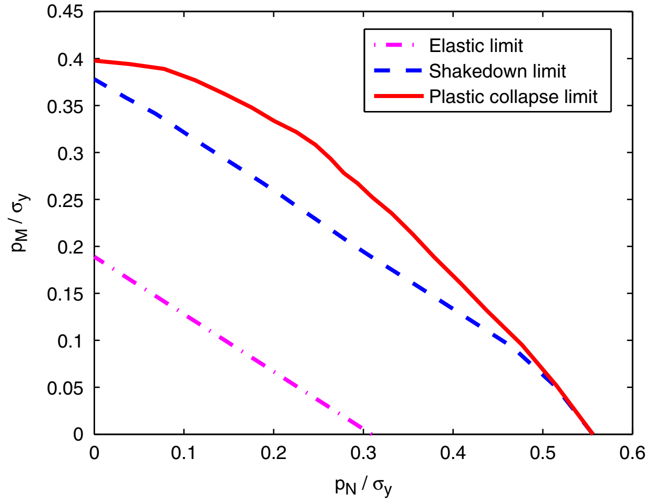

Figure 5. Interaction diagram of the grooved rectangular plate.

limit analysis, all the two bounds converge rapidly to the solution $\alpha_l = 0.27811$. Numerical result gives the shakedown load factor $\alpha_{sd} = 0.23603$ compared with 0.23494 obtained by Vu [47].

The interaction diagram of the plate in Figure 5 shows three limit lines: the plastic collapse limit, shakedown limit and elastic limit. It is observed that if bending is rather small, inadaptation will occur due to incremental plasticity. In other cases, the plastic fatigue dominates the inadaptation process. These results agree well with the solutions obtained by Vu [47] and Heitzer [46].

5.2. Square plate with a central circular hole

In this continuous well-known example, a square plate with central circular hole (Figure 6(a)) subjected to two loads p_1 and p_2 which can vary independently is considered. The limit load of the problem was obtained analytically by Gaydon and McCrum [49] by using plane stress hypothesis and von Mises yield criterion. Numerical limit and shakedown analyses were also investigated by some authors, e.g. Garcea *et al.* [9] for the case of $R/L = 0.2$ and Heitzer [46], Vu [47], Tran [48] for different ratios of R/L to evaluate the elastic–plastic behaviour of the structure.

In our analysis, due to the symmetry, one fourth of the plate is modelled and discretized by 288 T3 elements as shown in Figure 6(b). The two following cases are examined

One applied load. In this case one load is set to zero and the other one can vary within a range of $p_2 = 0$, $p_1 \in [0, \sigma_y]$. With $0 < R/L \leqslant 0.204$, the exact plastic collapse limit is found since the lower and the upper bounds are coincident in this range

$$p_{\lim} = (1 - R/L)\sigma_y. \tag{29}$$

As an example, the exact collapse limit load in the case of $R/L = 0.2$ is $p_{\lim} = 0.8\sigma_y$. Our numerical solutions obtained in this case are $0.79536\sigma_y$ as lower bound and $0.79801\sigma_y$ as upper bound. Based on an elastic analysis, the alternating (plastic fatigue) limit can be estimated. The

DOI: 10.1002/nme

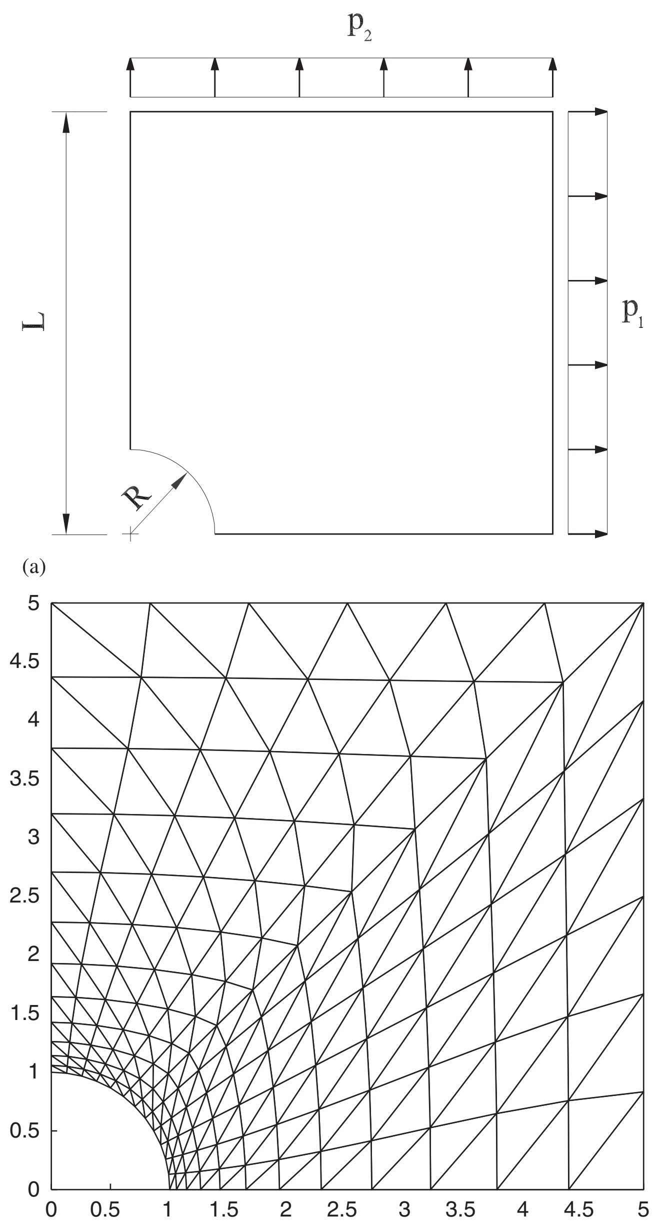

(a)

(b)

Figure 6. FE-mesh and geometrical dimensions of square plate.

DOI: 10.1002/nme

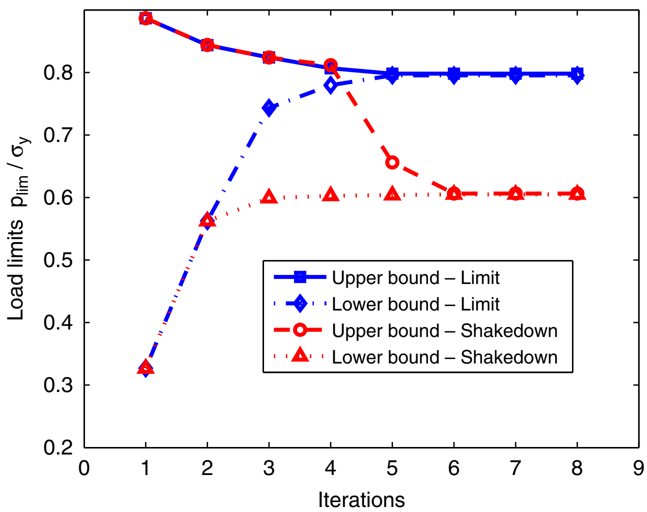

Figure 7. Square plate: convergence of limit and shakedown load factors.

Table II. Limit and shakedown load factors: $p_1 \in [0, \sigma_y]$, $p_2 = 0$.

	Limit analysis			Shakedown analysis		
R/L	[46]	[48]	Present	[46]	[48]	Present
0.1	0.8951	0.90172	0.89317	0.671	0.6546	0.65992
0.2	0.7879	0.80149	0.79669	0.6157	0.60332	0.60074
0.3	0.691	0.70221	0.69301	0.5212	0.52012	0.52525
0.4	0.572	0.59139	0.57598	0.4361	0.43367	0.43124
0.5	0.4409	0.40117	0.40112	0.3302	0.31600	0.32111
0.6	0.2556	0.24249	0.24286	0.2104	0.21323	0.21191
0.7	0.1378	0.12541	0.12774	0.1327	0.12378	0.12678
0.8	0.0565	0.05227	0.05212	0.0557	0.05225	0.05206
0.9	0.0193	0.01226	0.01326	0.0191	0.01226	0.01325

numerical results obtained by our shakedown algorithm represent the minimum between the alternating limit and the incremental limit. For $R/L = 0.2$, the collapse mode is alternating plasticity. Our obtained alternating limit is $0.59776\sigma_y$. The shakedown algorithm gives $0.59735\sigma_y$ as lower bound and $0.60423\sigma_y$ as upper bound. The convergence property of these solutions presented in Figure 7 shows that the limit and shakedown load factors become stationary after only five or six iteration steps.

In order to examine the geometric effect of the circular hole, various values of ratio R/L are also considered. The obtained numerical results are introduced in Table II, compared with the solutions of Heitzer [46], which were obtained by using lower bound method and eight-node elements (FEM-Q8) and with the solutions of Tran [48], which were obtained by using upper bound method and four-node plate elements. It can be observed that the present solutions agree well with those in [46, 48].

Table III. Limit analysis: $p_1 = p_2 = \sigma_y$.

R/L	Lower bound (analytical)	Upper bound (analytical)	Lower bound [47]	Upper bound [47]	Lower bound (present)	Upper bound (present)
0.1	0.97063	0.99215	0.97082	0.97104	0.97074	0.97102
0.2	0.89425	0.92376	0.89374	0.89472	0.89401	0.89765
0.3	0.79122	0.80829	0.79075	0.79125	0.79069	0.79102
0.4	0.67602	0.69048	0.67585	0.67592	0.67530	0.67654
0.5	0.55682	0.55682	0.55666	0.55679	0.55680	0.55690
0.6	0.43801	0.43801	0.43791	0.43819	0.43790	0.43828
0.7	0.32195	0.32195	0.32196	0.32221	0.32189	0.32207
0.8	0.20991	0.20991	0.21010	0.21016	0.21001	0.21008
0.9	0.10249	0.10249	0.10264	0.10267	0.10255	0.10254

Table IV. Shakedown analysis: $p_1 \in [0, \sigma_y]$, $p_2 \in [0, \sigma_y]$, two-parameter loads.

R/L	Alternating limit [47]	Lower bound [47]	Upper bound [47]	Alternating limit (present)	Lower bound (present)	Upper bound (present)
0.1	0.49082	0.49082	0.49086	0.48805	0.48800	0.48919
0.2	0.43384	0.43384	0.43390	0.43402	0.43399	0.43409
0.3	0.36128	0.36128	0.36131	0.36246	0.36244	0.36250
0.4	0.27635	0.27635	0.27638	0.27672	0.27672	0.27683
0.5	0.19442	0.19442	0.19445	0.19466	0.19466	0.19472
0.6	0.12360	0.12360	0.12364	0.12364	0.12364	0.12385
0.7	0.06763	0.06763	0.06765	0.06754	0.06754	0.06783
0.8	0.02903	0.02903	0.02905	0.02953	0.02953	0.02984
0.9	0.00709	0.00709	0.00710	0.00721	0.00721	0.00753

Two applied loads. For this case, exact value of the plastic collapse limit load are known in the range $0.483 < R/L \leqslant 1$ where analytical lower bound coincides with upper one

$$p_{\lim} = \frac{2}{\sqrt{3}} \sin\left(\alpha - \frac{\pi}{6}\right) \sigma_y, \quad \frac{1}{(R/L)^2} = \frac{\sqrt{3}}{2\cos(\alpha)} \mathrm{e}^{\sqrt{3}(\alpha - \pi/6)}. \tag{30}$$

Details about the upper and lower bounds within the range $0 \leqslant R/L < 0.483$ can be found in the work of Gaydon and McCrum [49]. Numerical limit and shakedown load factors for different values of R/L are introduced in Tables III and IV, compared with analytical results in [49] and numerical results in [47]. It can be seen that present results match well with the analytical solutions for limit analysis. The maximum error is less than 1%.

Table V shows a comparison between our numerical solutions with others obtained by different FEM discretization and solution strategies for $R/L = 0.2$. Figure 8 presents the interaction diagram of limit and shakedown analyses for the case of $R/L = 0.2$. It is observed that the shakedown loads are symmetric via p_1/σ_y- axis, i.e. they are the same for both positive and negative ranges of p_2, while the plastic collapse limits are not. It is also noted that when one load varies within the negative range, the collapse mode is purely alternating plasticity as shown in Tran [48].

Table V. Limit and shakedown analysis: comparison.

	Limit analysis			Shakedown analysis		
(p_1, p_2)	(1, 1)	(1, 0.5)	(1, 0)	(1, 1)	(1, 0.5)	(1, 0)
Belytschko [50]	—	—	0.780	0.431	0.501	0.571
Corradi *et al.* [51]	0.767	—	0.691	0.504	0.579	0.654
Genna [52]	—	—	0.793	0.478	0.566	0.653
Stein and Zhang [53]	—	—	0.802	0.453	0.539	0.624
Zhang *et al.* [54]	0.893	0.907	0.789	0.477	0.549	0.647
Gross-Wedge [55]	0.882	0.891	0.782	0.446	0.524	0.614
Zouanin [56]	0.894	0.911	0.803	0.429	0.500	0.594
Garcea *et al.* [9]	0.902	0.912	0.806	0.438	0.508	0.604
Present	0.896	0.905	0.797	0.434	0.505	0.601

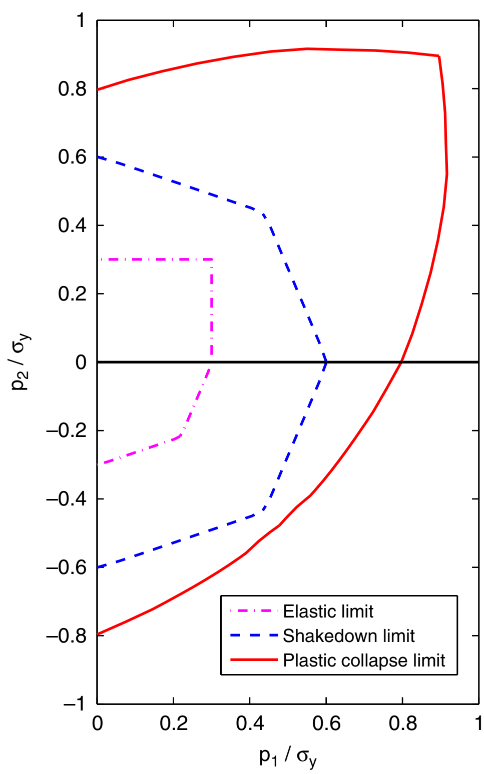

Figure 8. Square plate: interaction diagram of a square plate with a central hole, $R/L = 0.2$.

5.3. Simple frame

In this example, we investigate a simple frame depicted in Figure 9(a) subjected to two loads p_1 and p_2 which can vary independently. Two different boundary conditions are considered: (a) only the horizontal displacement on the left boundary is free and (b) both vertical and horizontal

DOI: 10.1002/nme

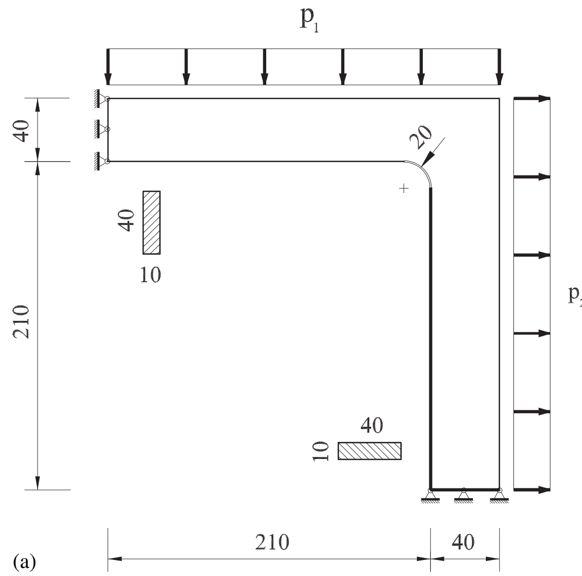

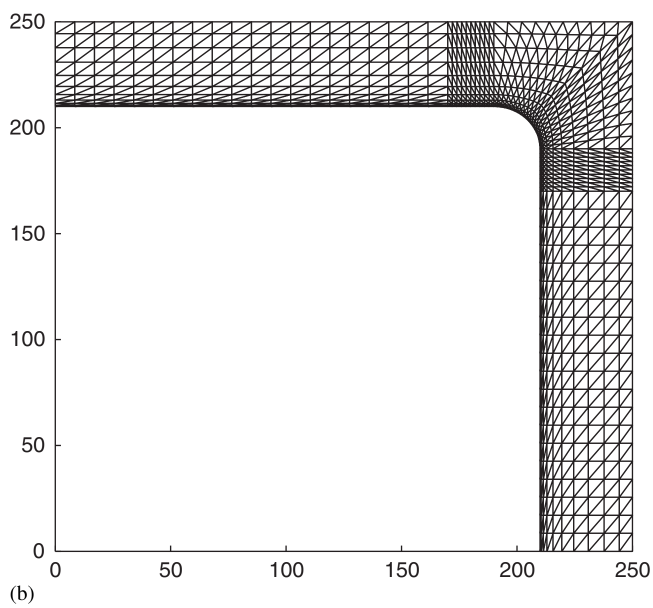

Figure 9. FE-mesh and geometrical dimensions of simple frame.

displacements on both boundaries are fixed. This example was studied in [9] by using an iterative method, which is based on a mixed triangular finite element and a piecewise linearization of the elastic domain. For the purpose of comparison, the load domain, geometrical data and material properties are chosen analogously as in [9], i.e. $p_1 \in [1.2, 3.0]$, $p_2 \in [0.4, 1.0]$, $E = 2.10^5$, $v = 0.3$, $\sigma_y = 10$. The frame is discretized by 1600 T3 elements as shown in 9(b).

DOI: 10.1002/nme

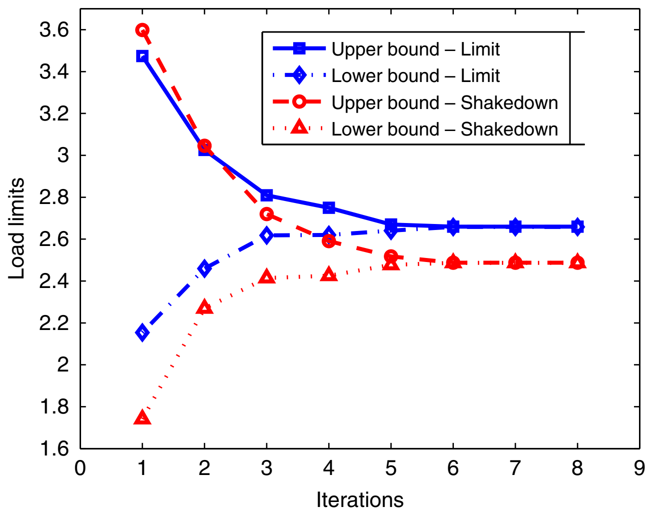

Figure 10. Simple frame: convergence of limit and shakedown load factors.

Table VI. Limit analysis: comparison.

	Garcea *et al.* [9]		Present	
(p_1, p_2)	(a)	(b)	(a)	(b)
(1.2, 1.0)	2.975	7.804	2.970	7.901
(3.0, 0.4)	2.831	4.207	2.792	4.241
(3.0, 1.0)	2.645	3.949	2.659	4.008

Table VII. Shakedown analysis: comparison.

	Garcea *et al.* [9]		Present	
Limits	(a)	(b)	(a)	(b)
Elastic	1.203	1.355	1.192	1.427
Alternating	2.940	4.518	2.922	4.657
Ratcheting	2.473	3.925	2.487	4.006

Figure 10 shows the evolutions of limit and shakedown load factors for case (a). In the case of limit analysis with $p_1 = 3.0$, $p_2 = 1.0$, all the two bounds converge rapidly to the solution $\alpha_l = 2.659$. Numerical result gives the shakedown load factor $\alpha_{sd} = 2.487$ compared with 2.473 obtained by Garcea *et al.* [9]. Tables VI and VII show a comparison between our numerical results for limit and shakedown analysis with those obtained in [9]. It is observed that for both cases (a) and (b), inadaptation will occur due to incremental plasticity (ratcheting) as already pointed out in [9].

DOI: 10.1002/nme

6. CONCLUSIONS

A numerical procedure for limit and shakedown analyses of structures using a novel ES-FEM has been first presented in this study. The procedure involves a primal–dual algorithm based upon the von Mises yield criterion and a Newton method to determine simultaneously both the upper and lower bounds of the plastic collapse limit and the shakedown limit. Using constant smoothing function, only one Gaussian point is required for each domain ensuring that the total number of variables in the resulting optimization problem is kept to a minimum compared with standard finite element formulation. The actual Newton directions are updated at each iteration by solving a purely-elastic-like system of linear equations to ensure the kinematical condition of the displacements to be satisfied automatically.

The obtained solutions match well with analytical values and show remarkably good performance compared with the results of several other numerical methods in the literature. At each iteration, the lower bound is calculated coupling with the upper bound with no extra computational cost. This calculation will provide a useful tool to estimate the accuracy of the solution and to ensure the convergence of the proposed algorithm. A very effective numerical method is achieved due to the lesser computational cost by using constant smoothing domains constructed on edges of elements and by direct plasticity methods that achieve plastic solutions in the computing time of only 4–5 linear elastic steps. On the other hand, by using the Newton iterative method, the problem size is reduced to the size of linear elastic analysis, and hence there is no limit in practical applications.

ACKNOWLEDGEMENTS

This work is partially supported by A*Star, Singapore (SERC Grant No: 052 101 0048). It is also partially supported by the Open Research Fund Program of the State Key Laboratory of Advanced Technology of Design and Manufacturing for Vehicle Body, Hunan University, P.R.China under the grant number 40915001.

REFERENCES

1. Bree J. Elastic–plastic behaviour of thin tubes subjected to internal pressure and intermittent high-heat fluxes with applications to fast-nuclear-reactor fuel elements. *Journal of Strain Analysis* 1967; **2**:226–238.
2. Tran TN, Kreißig R, Staat M. Probabilistic limit and shakedown analysis of thin shells. *Structural Safety* 2009; **31**(1):1–18.
3. Tran TN, Kreißig R, Vu DK, Staat M. Upper bound limit and shakedown analysis of shells using the exact Ilyushin yield surface. *Computers and Structures* 2008; **86**(17–18):1683–1695.
4. Heitzer M, Staat M. FEM-computation of load carrying capacity of highly loaded passive components by direct methods. *Nuclear Engineering and Design* 1999; **193**(3):349–358.
5. Krabbenhoft K, Damkilde L. A general non-linear optimization algorithm for lower bound limit analysis. *International Journal for Numerical Methods in Engineering* 2003; **56**:165–184.
6. Andersen KD, Christiansen E, Conn AR, Overton ML. An efficient primal–dual interior-point method for minimizing a sum of Euclidean norms. *SIAM Journal on Scientific Computing* 2000; **22**:243–262.
7. Vu DK, Yan AM, Nguyen DH. A primal–dual algorithm for shakedown analysis of structure. *Computer Methods in Applied Mechanics and Engineering* 2004; **193**:4663–4674.
8. Vu DK, Staat M, Tran IT. Analysis of pressure equipment by application of the primal–dual theory of shakedown. *Communications in Numerical Methods in Engineering* 2007; **23**(3):213–225.
9. Garcea G, Armentano G, Petrolo S, Casciaro R. Finite element shakedown analysis of two-dimensional structures. *International Journal for Numerical Methods in Engineering* 2005; **63**:1174–1202.
10. Chen JS, Wu CT, Yoon S, You Y. A stabilized conforming nodal integration for Galerkin mesh-free methods. *International Journal for Numerical Methods in Engineering* 2001; **50**:435–466.

11. Rabczuk T, Belytschko T, Xiao SP. Stable particle methods based on Lagrangian kernels. *Computer Methods in Applied Mechanics and Engineering* 2004; **193**(12–14):1035–1063.
12. Rabczuk T, Belytschko T. Cracking particles: a simplified meshfree method for arbitrary evolving cracks. *International Journal for Numerical Methods in Engineering* 2004; **61**(13):2316–2343.
13. Rabczuk T, Areias PMA. A meshfree thin shell for arbitrary evolving cracks based on an external enrichment. *Computer Modeling in Engineering and Sciences* 2006; **16**(2):115–130.
14. Rabczuk T, Areias PMA, Belytschko T. A meshfree thin shell method for non-linear dynamic fracture. *International Journal for Numerical Methods in Engineering* 2007; **72**(5):524–548.
15. Liu GR, Zhang GY, Wang YY, Huang HT, Zhong ZH, Li GY, Han X. A linearly conforming point interpolation method (LC-PIM) for three-dimensional elasticity problems. *International Journal for Numerical Methods in Engineering* 2007; **72**:1524–1543.
16. Liu GR, Zhang GY, Wang YY, Huang HT, Zhong ZH, Li GY, Han X. A linearly conforming point interpolation method (LC-PIM) for three-dimensional elasticity problems. *International Journal for Numerical Methods in Engineering* 2007; **72**:1524–1543.
17. Liu GR, Li Y, Dai KY, Luan MT, Xue W. A linearly conforming radial point interpolation method for solid mechanics problems. *International Journal of Computational Methods* 2006; **3**(4):401–428.
18. Liu GR, Nguyen-Thoi T, Nguyen-Xuan H, Dai KY, Lam KY. On the essence and the evaluation of the shape functions for the smoothed finite element method (SFEM) (Letter to Editor). *International Journal for Numerical Methods in Engineering* 2009; **77**:1863–1869.
19. Hung NX, Stephane B, Hung ND. Smooth finite element methods: convergence, accuracy and properties. *International Journal for Numerical Methods in Engineering* 2008; **74**:175–208.
20. Liu GR, Nguyen-Thoi T, Nguyen-Xuan H, Lam KY. A node-based smoothed finite element method (NS-FEM) for upper bound solutions to solid mechanics problems. *Computers and Structures* 2009; **87**:14–26.
21. Liu GR, Dai KY, Nguyen-Thoi T. A smoothed finite element for mechanics problems. *Computational Mechanics* 2007; **39**:859–877.
22. Liu GR, Nguyen-Thoi T, Dai KY, Lam KY. Theoretical aspects of the smoothed finite element method (SFEM). *International Journal for Numerical Methods in Engineering* 2007; **71**:902–930.
23. Dai KY, Liu GR, Nguyen-Thoi T. An *n*-sided polygonal smoothed finite element method (nSFEM) for solid mechanics. *Finite Elements in Analysis and Design* 2007; **43**:847–860.
24. Dai KY, Liu GR. Free sand forced vibration analysis using the smoothed finite element method (SFEM). *Journal of Sound and Vibration* 2007; **301**:803–820.
25. Nguyen-Thoi T, Liu GR, Dai KY, Lam KY. Selective smoothed finite element method. *Tsinghua Science and Technology* 2007; **12**(5):497–508.
26. Nguyen-Xuan H, Bordas S, Nguyen-Dang H. Addressing volumetric locking and instabilities by selective integration in smoothed finite elements. *Communications in Numerical Methods and Engineering* 2008; **25**:19–34.
27. Nguyen-Xuan H, Rabczuk T, Bordas S, Debongnie JF. A smoothed finite element method for plate analysis. *Computer Methods in Applied Mechanics and Engineering* 2008; **197**:1184–1203.
28. Nguyen-Thanh N, Rabczuk T, Nguyen-Xuan H, Bordas S. A smoothed finite element method for shell analysis. *Computer Methods in Applied Mechanics and Engineering* 2008; **198**:165–177.
29. Nguyen-Xuan H, Nguyen-Thoi T. A stabilized smoothed finite element method for free vibration analysis of Mindlin–Reissner plates. *Communications in Numerical Methods in Engineering* 2009; **25**:882–906.
30. Cui XY, Liu GR, Li GY, Zhao X, Nguyen-Thoi T, Sun GY. A smoothed finite element method (SFEM) for linear and geometrically nonlinear analysis of plates and shells. *CMES—Computer Modeling in Engineering and Sciences* 2008; **28**(2):109–125.
31. Bordas S, Rabczuk T, Nguyen-Xuan H, Nguyen Vinh P, Natarajan S, Bog T, Do Minh Q, Nguyen Vinh H. Strain smoothing in FEM and XFEM. *Computers and Structures* 2008; DOI: 10.1016/j.compstruc.2008.07.006.
32. Nguyen-Thoi T, Liu GR, Nguyen-Xuan H, Nguyen-Tran C. Adaptive analysis using the node-based smoothed finite element method (NS-FEM). *Communications in Numerical Methods in Engineering* 2009; DOI: 10.1002/cnm.1291.
33. Liu GR, Nguyen-Thoi T, Lam KY. A novel alpha finite element method (αFEM) for exact solution to mechanics problems using triangular and tetrahedral elements. *Computer Methods in Applied Mechanics and Engineering* 2008; **197**:3883–3897.
34. Liu GR, Nguyen-Thoi T, Lam KY. An edge-based smoothed finite element method (ES-FEM) for static, free and forced vibration analyses of solids. *Journal of Sound and Vibration* 2009; **320**:1100–1130.

35. Nguyen-Xuan H, Liu GR, Nguyen-Thoi T, Nguyen Tran C. An edge-based smoothed finite element method (ES-FEM) for analysis of two-dimensional piezoelectric structures. *Smart Materials and Structures* 2009; DOI: stacks.iop.org/SMS/18/000000.
36. Nguyen-Thoi T, Liu GR, Lam KY. A face-based smoothed finite element method (FS-FEM) for 3D linear and nonlinear solid mechanics problems using 4-node tetrahedral elements. *International Journal for Numerical Methods in Engineering* 2009; **78**(3):324–353.
37. Nguyen-Thoi T, Liu GR, Vu-Do HC, Nguyen-Xuan H. A face-based smoothed finite element method (FS-FEM) for visco-elastoplastic analyses of 3D solids using tetrahedral mesh. *Computer Methods in Applied Mechanics and Engineering* 2009; DOI: 10.1016/j.cma.2009.07.001.
38. Arnold DN. Mixed finite element methods for elliptic problems. *Computer Methods in Applied Mechanics and Engineering* 1990; **82**:281–300.
39. Mijuca D, Berkovic M. On the efficiency of the primal-mixed finite element scheme. *Advances in Computational Structured Mechanics*; *Civil-Comp Press* 1998; 61–69.
40. Rong TY, Lu AQ. Generalized mixed variational principles and solutions for ill-conditioned problems in computational mechanics: Part I. Volumetric locking. *Computer Methods in Applied Mechanics and Engineering* 2001; **191**:407–422.
41. Rong TY, Lu AQ. Generalized mixed variational principles and solutions for ill-conditioned problems in computational mechanics: Part II. Shear locking. *Computer Methods in Applied Mechanics and Engineering* 2003; **192**:4981–5000.
42. Vu DK, Yan AM, Nguyen DH. A dual form for discretized kinematic formulation in shakedown analysis. *International Journal of Solids and Structures* 2004; **41**:267–277.
43. Prager W, Hodge Jr PG. *Theory of Perfectly Plastic Solids*. Wiley: New York, 1951.
44. Casciaro R, Cascini L. A mixed formulation and mixed finite elements for limit analysis. *International Journal for Numerical Methods in Engineering* 1982; **18**:211–243.
45. Yan AM. Contribution to the direct limit state analysis of plastified and cracked structures. *Dissertation*, Université de Liège, Belgium, 1997.
46. Heitzer M. Traglast- und Einspielanalyse zur Bewertung der Sicherheit passiver Komponenten. *Berichte des Forschungszentrums Jülich*, Jül-3704, *Dissertation*, RWTH Aachen, Germany, 1999.
47. Vu DK. Dual limit and shakedown analysis of structures. *Dissertation*, Université de Liège, Belgium, 2001.
48. Tran TN. Limit and shakedown analysis of plates and shells including uncertainties. *Dissertation*, Technische Universität Chemnitz, Germany, 2008. Available from: http://archiv.tu-chemnitz.de/pub/2008/0025.
49. Gaydon FA, McCrum AW. A theoretical investigation of the yield point loading of a square plate with a central circular hole. *Journal of the Mechanics and Physics of Solids* 1954; **2**:156–169.
50. Belytschko T. Plane stress shakedown analysis by finite element. *International Journal of Mechanical Sciences* 1972; **14**:619–625.
51. Corradi L, Zavelani A. A linear programming approach to shakedown analysis of structures. *Computer Methods in Applied Mechanics and Engineering* 1974; **3**:37–53.
52. Genna F. A non-linear inequality, finite element approach to the direct computation of the shakedown load safety factor. *International Journal of Mechanical Sciences* 1988; **30**:769–789.
53. Stein E, Zhang G. Shakedown with non-linear strain-hardening including structural computation using finite element method. *International Journal of Plasticity* 1992; **8**:1–31.
54. Zhang X, Liu Y, Cen Z. Boundary element methods for lower bound limit and shakedown analysis. *Engineering Analysis of Boundary Methods* 2004; **28**:905–917.
55. Gross-Wedge J. On the numerical assessment of the safety factor of elastic–plastic structures under variable loading. *International Journal of Mechanical Sciences* 1997; **39**(4):417–433.
56. Zouanin N, Borges L, Silveira JL. An algorithm for shakedown analysis non-linear yield function. *Computer Methods in Applied Mechanics and Engineering* 2002; **191**:2463–2481.